Desalination and Water Treatment 317 (2024) 100278

Contents lists available at ScienceDirect

Desalination and Water Treatment

journal homepage: www.sciencedirect.com/journal/desalination-and-water-treatment/

Valorization of *Silybum marianum* seed shells waste as biosorbent for basic fuchsin dye removal from water: kinetics, isotherms, and thermodynamic studies

Atef Ali Ahmed[a,b], Zhour Hattab[b,*], Yamina Berredjem[b], Souaad Hamoudi[c,d], Ridha Djellabi[e]

[a] *Laboratory of Physics matter and Radiation, Department of Process Engineering, Faculty of Science and Technology, University Mohammed Cherif Messaadia, Souk-Ahras, Algeria*
[b] *Laboratory of Water Treatment and Valorization of Industrial Wastes, Department of Chemistry, Faculty of Science, University Badji Mokhtar, Annaba, Algeria*
[c] *Laboratory of Materials Technology and Process Engineering, Faculty of Exact Sciences, University of Bejaia, Algeria*
[d] *Department of Chemistry, Faculty of Science, University Badji Mokhtar, Annaba, Algeria*
[e] *Departament d'Enginyeria Química, Universitat Rovira i Virgili, Av Països Catalans 26, 43007 Tarragona, Spain*

ARTICLE INFO

Keywords:
Silybum marianum
Basic fuchsin
Adsorption
Water treatment
Wastes valorization

ABSTRACT

Over the last decades, the valorization of agro-industrial wastes into adsorbents has received a lot of attention due to the low-cost, high performance and sustainability factors. This work aims to valorize *Silybum marianum* seed shells (SMSS) as biosorbent for the removal of basic fuchsin dye (BF) from water. The prepared biosorbent from SMSS was characterized to check the morphological and structural proprieties using several techniques including FTIR, XRD, SEM, TGA-DTA, and BET. It was found that SMSS has a fibrous semi-amorphous structure typical of lignocellulosic materials. The study also investigated the impact of numerous operational parameters on basic fuchsin biosorption efficiency, including particle size, biosorbent mass, stirring speed, initial dye concentration, temperature, and pH of solution. Additionally, the research explored the influence of natural water matrices on dye removal. The adsorption performance was found to be higher at basic pH values, reaching 97.50%. The adsorption process was analyzed using different kinetic models, and it was found that the process follows a pseudo-second-order model. The experimental data was thoroughly scrutinized using the Freundlich and Langmuir isotherm models. The results confirm that Langmuir model fits well the BF dye adsorption on SMSS surface. The thermodynamic study revealed that the adsorption process of BF dye onto SMSS was endothermic. Overall, SMSS shows great adsorption ability which might be a good candidate for real wastewater treatment, by considering low-cost and availability of the original waste.

1. Introduction

Dyes have played an essential role in industrial and daily applications, serving a variety of purposes such as coloring cloth, leather, and hair, as well as acting as food pigments. Due to recent economic growth and population increase, the demand for synthetic dyes has surged dramatically. As consequence, the excessive use of dyes in various industries has led to severe pollution of surface and groundwater. The highly contaminated wastewaters released by various industries poses an environmental and health threat due to the toxicity and complex aromatic structures of dyes [1]. This makes them challenging to decompose, leaving visible colored substances in lakes and rivers that make water unfit for human consumption [2]. Over the last decades, several approaches for water treatment including dye removal have been integrated in industrial scale [3], including chemical/electrochemical precipitation [4,5], membrane filtration [6], coagulation/flocculation [7], and photocatalysis [8]. However, adsorption has proven to be the most cost-effective method for removing organic pollutants from water [9]. Within the context of circular economy which recommends the valorization or/and recycling of wastes into valuable products, current research has given a special attention to develop materials from agro-wastes for water treatment, owing their low-cost and large worldwide availability [10,11]. In fact, the adsorption abilities of adsorbents obtained from wastes valorization have shown various performances towards different pollutants. The characteristics of wastes based on their origin as well as the synthesis process have crucial roles for obtaining highly sportive materials. Herein, this study aims to estimate the ability of *Silybum marianum* seed shells

* Corresponding author.
E-mail address: zoumourouda20012000@yahoo.fr (Z. Hattab).

https://doi.org/10.1016/j.dwt.2024.100278
Received 16 January 2024; Received in revised form 16 January 2024; Accepted 15 February 2024

Nomenclature

R	The removal efficiency (%).
C_0	Initial dye concentrations (mg/L).
C_t	Current dye concentrations (mg/L).
q_e	Amount of dye adsorbed at equilibrium (mg/g).
q_t	Amount of dye adsorbed at time t (mg/g).
K_1	The pseudo-first-order rate constant (1/min).
K_2	The pseudo-second-order rate constant (g/mg.min).
K_f	The first coefficient of the Freundlich equation (L/mg).
K_L	The Langmuir kinetic constant (L/mg).
n	The second coefficient of Freundlich equation.
q_m	The maximum adsorption capacity (mg/g).
C_e	Dye concentration at equilibrium (mg/L).
Kc	The equilibrium adsorption constant (L/mg).
R	The universal gas constant (8.314 J/mol.K).
T	The absolute temperature (K).

(SMSS) as an adsorbent for dye removal from water. SMSS is highly available in Mediterranean region and it is considered to be a weed and known for its medicinal properties. This readily available bio-waste has remained unexplored in the water treatment field. SMSS was valorized into adsorbent powder and used for the removal of BF dye from water under different conditions in batch system. Several parameters were studies such as particle size, biosorbent mass, stirring speed, initial dye concentration, temperature, and solution pH. The mechanisms behind the effect of these factors on SMSS adsorption behavior were discussed in depth. SMSS used in this study was not subjected to any chemical modification. Adsorption kinetics data were analyzed by two main models, i.e., pseudo-first-order and pseudo-second-order. Meanwhile, the equilibrium isotherms data were modeled using Freundlich and Langmuir equations. The thermodynamic parameters for BF ions adsorption were also determined.

2. Materials and methods

2.1. Dye preparation

The Basic fuchsin dye ($C_{20}H_{20}ClN_3$) utilized in this research was acquired from Sigma-Aldrich-Fluka, located in Saint-Quentin, Fallavier, France. A stock solution was prepared by dissolving 1 g of Basic fuchsin in 1 L of distilled water, and subsequent dilution was performed to obtain colored solutions with different concentrations (10, 20, 30, and 40 mg/L).

2.2. Biosorbent preparation

Silybum marianum seeds were obtained from a farm in the Souk Ahras province of eastern Algeria. In order to separate the core from the shells, the seeds were grounded and washed multiple times with distilled water, utilizing a magnetic stirrer for assistance. Excess moisture was eliminated by drying the seed shells in an oven set to 105 °C overnight. Finally, *Silybum marianum* seed shells (SMSS) were sieved to obtain various particle sizes.

2.3. Characterization of SMSS

The functional groups of SMSS before and after adsorption were identified using Fourier Transform Infrared (FTIR) analysis which was carried out on IR Affinity-1S (SHIMADZU), employing a single reflection ATR. FTIR patterns were recorded at a maximum pressure of 0.1 GPa, with a standard resolution of 4 cm^{-1} and an accumulation of 50. Additionally, XRD spectra were acquired using a Rigaku Miniflex diffractometer equipped with a CuKa radiation source (λ = 1.5418 Å), scanning within the range of 10 to 80°. The morphology of SMSS was further examined through scanning electron microscopy (SEM) using Quanta FEG 250 instrument. Furthermore, the thermal analysis of SMSS was conducted via TGA and DTA using the STA PT1600 LINSEIS apparatus. The measurements were conducted under a nitrogen atmosphere with a heating rate of 10 °C/min in the temperature range of 50–800 °C. BET surface area analysis was performed with nitrogen gas at 77.3 K, utilizing QuadraSorb Station 2 version 5.04.

2.4. Adsorption experiments

A sequence of batch experiments was undertaken to evaluate the impact of various factors on adsorption efficiency. In each experiment, a specific amount of SMSS was added to 250 mL conical flasks containing 100 mL of dye solution, and stirred for one hour. At given intervals, the residual concentration of BF dye was assessed using a UV-Vis spectrophotometer at 550 nm. The presented results are the average of three replicated experiments. The pH factor was manipulated using either HCl (0.1 M) or NaOH (0.1 M). The removal efficiency (R %) was calculated utilizing the provided Eq. (1).

$$\mathbf{R}(\%) = \frac{\mathbf{C_0 - C_t}}{\mathbf{C_0}} \quad \mathbf{x} \quad \mathbf{100} \tag{1}$$

C_0 denotes the initial concentration, while C_t represents concentration of the colored solution at time t.

2.5. Adsorption kinetics

The kinetics of adsorption plays a determinant role in the schematic representation of the adsorption process and the optimization of experimental parameters influencing adsorbent-adsorbate interactions. The experimental data, acquired for different times and initial dye concentrations, were subjected to pseudo-first-order and pseudo-second-order models to enhance the comprehension of the adsorption mechanism concerning BF dye. Under the pseudo-first-order kinetic model, the reaction rate is directly proportional to the difference between the equilibrium concentration and the instantaneous concentration of the material in a solid phase [12], as expressed through Eq. (2). Conversely, the rate of the pseudo-second-order reaction is contingent upon the adsorbed quantity by the material and the adsorbed quantity at equilibrium [13], as articulated in Eq. (3).

$$\frac{\mathbf{dq_t}}{\mathbf{q_t}} = \mathbf{K_1(q_e - q_t)} \tag{2}$$

$$\frac{\mathbf{dq_t}}{\mathbf{q_t}} = \mathbf{K_2(q_e - q_t)^2} \tag{3}$$

Where q_e and q_t denote the quantities of dye adsorbed at equilibrium and time t (mg/g), while K_1 represents the rate constant associated with the pseudo-first-order model (1/min), and K_2 refers to the rate constant of the pseudo-second-order model (g/mg.min).

2.6. Adsorption isotherms

Two common models are often used to elucidate adsorption isotherm data, namely the Freundlich and Langmuir models. The empirical Freundlich model, introduced in 1926 [14], posits the heterogeneity of the adsorbent surface and envisions a multilayer adsorption process. This model is expressed by Eq. (4). On the other hand, the Langmuir model assumes that the adsorption sites of the adsorbent are uniform and that the adsorption is monolayer. The Langmuir model is represented by Eq. (5) [15].

$$\mathbf{lnq_e = lnK_f + \frac{1}{n} lnC_e} \quad (4)$$

$$\mathbf{\frac{C_e}{q_e} = \frac{1}{q_m} Ce + \frac{1}{K_L q_m}} \quad (5)$$

K_f represents the Freundlich equation's first coefficient (L/mg), while K_L refers to Langmuir kinetic constant (L/mg). n represents the second coefficient in the Freundlich equation, indicating the adsorption intensity. q_e refers to the adsorbed amount at equilibrium (mg/g), and q_m denotes the maximum adsorption capacity (mg/g). The variable C_e represents the adsorbate concentration in the solution at equilibrium (mg/L).

2.7. Thermodynamic parameters

Investigating the influence of temperature is crucial in identifying the nature and spontaneity of the adsorption process [16]. The temperature dependency is associated with three pertinent thermodynamic parameters: the change in Gibb's free energy (ΔG°), the change in enthalpy (ΔH°), and the change in entropy (ΔS°). The Measurement of these parameters is achievable through the application of the subsequent equations [17]:

$$\mathbf{\Delta G^\circ = -R.\,T.\,LnKc} \quad (6)$$

$$\mathbf{\Delta G^\circ = \Delta H^\circ - T.\,\Delta S^\circ} \quad (7)$$

Where Kc is the equilibrium adsorption constant (L/mg), R represents the universal gas constant (8.314 J/mol.K), and T refers to absolute temperature (K).

3. Results and discussion

3.1. Characterizations

3.1.1. Structure analysis by FTIR

Fig. 1 displays the Fourier Transform Infrared (FTIR) spectra of SMSS both before and after adsorption, depicting several discernible peaks. Specifically, the peak observed at 2929 cm^{-1} is attributed to the C-H group within lignin, while the band at 2359 cm^{-1} is assigned to C-C. The band located at 1735 cm^{-1} corresponds to the C═O group of hemicelluloses, and the band at 1651 cm^{-1} corresponds to the C═C group. The C═O band originating from the aromatic lignin ring manifests at 1543 cm^{-1}. In addition, the band identified at 1256 cm^{-1} corresponds to C-O of lignin and xylene, and the band at 1015 cm^{-1} is associated with the C-OH group of hemicelluloses and cellulose [18]. The previously identified peaks exhibit a decrease in intensity and a positional shift after adsorption, indicating an interaction between the functional groups of BF dye and the surface of SMSS.

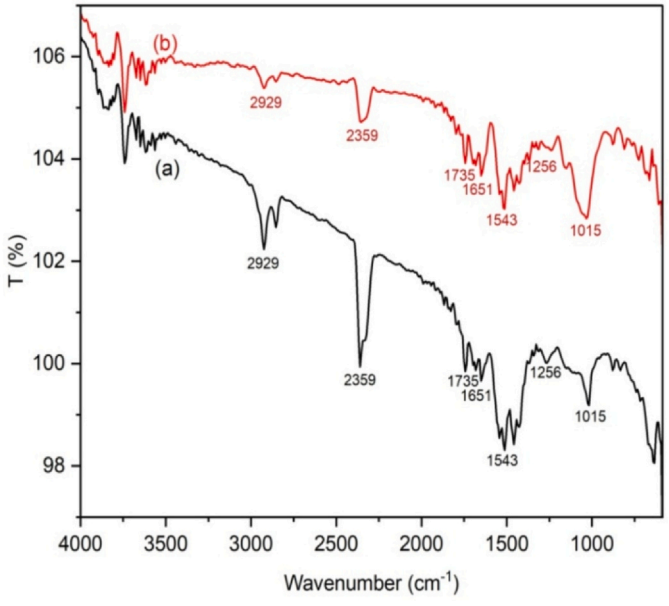

Fig. 1. FTIR spectra of Silybum marianum seed shells (a) before BF adsorption, and (b) after BF adsorption ([BF] = 10 mg/L; t = 60 min; SMSS particle size: [250 − 500] µm; [SMSS] = 5 g/L; Stirring speed = 150 rpm; Original pH = 6.9; T = 25 °C).

3.1.2. Structure analysis by XRD

Fig. 2 depicts the X-ray diffraction pattern of SMSS, showcasing a cellulosic material's characteristic spectrum. Notably, a dominant peak appears at 2θ = 22°, indicating the existence of a well-formed crystalline cellulose structure which is in agreement with FTIR spectra. On top of that, a lesser organized polysaccharide structure is revealed by secondary peaks. It can be concluded that SMSS exhibits a semi-amorphous structure.

3.1.3. SEM

The morphological structure of *Silybum marianum* seed shells at two different magnification levels is illustrated in Fig. 3. SMSS images show a fibrous structure typical of a lignocellulosic material. Furthermore, it was observed that the cell walls contain numerous small cavities, facilitating the transfer of chemical species in all directions within the cells. This characteristic is advantageous for the effective retention of dyes [19].

3.1.4. Thermal analysis by TGA-DTA

Thermal analysis of SMSS was investigated through Thermogravimetric Analysis (TGA) and Differential Thermal Analysis (DTA) spanning a temperature range of 50 to 800 °C. The weight of the sample employed for this analysis was 14.807 mg. The initiation of thermal degradation is discerned through a significant decrease in sample weight, indicative of exothermic combustion reactions [20]. The TGA and DTA curves of SMSS are shown in Fig. 4. Four distinctive stages of mass loss can be observed and distinguish the thermal transformation process. The first stage, observed between 50 and 120 °C, is attributed to the evaporation of surface water from SMSS. The second stage, ranging from 200 to 320 °C, corresponds to the thermal degradation of hemicelluloses. The third stage, from 320 to 400 °C, is associated with the degradation of cellulose. The last stage, from 400 to 800 °C, is due to the gradual decomposition of lignin, characterized by

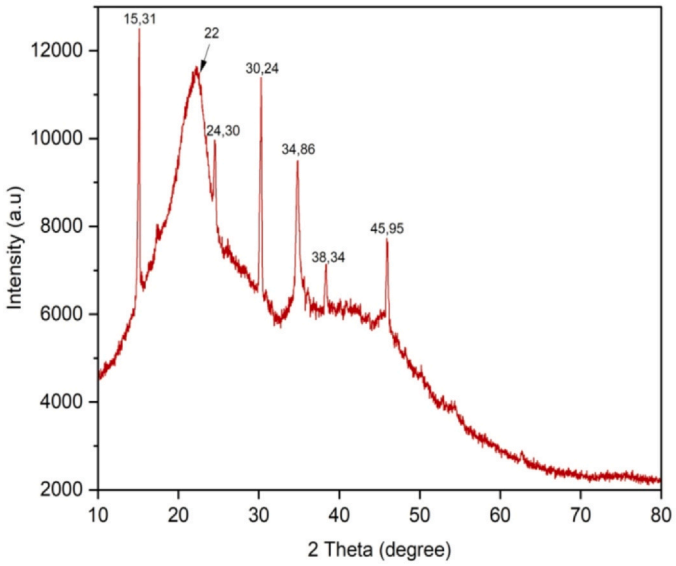

Fig. 2. XRD analysis of Silybum marianum seed shells.

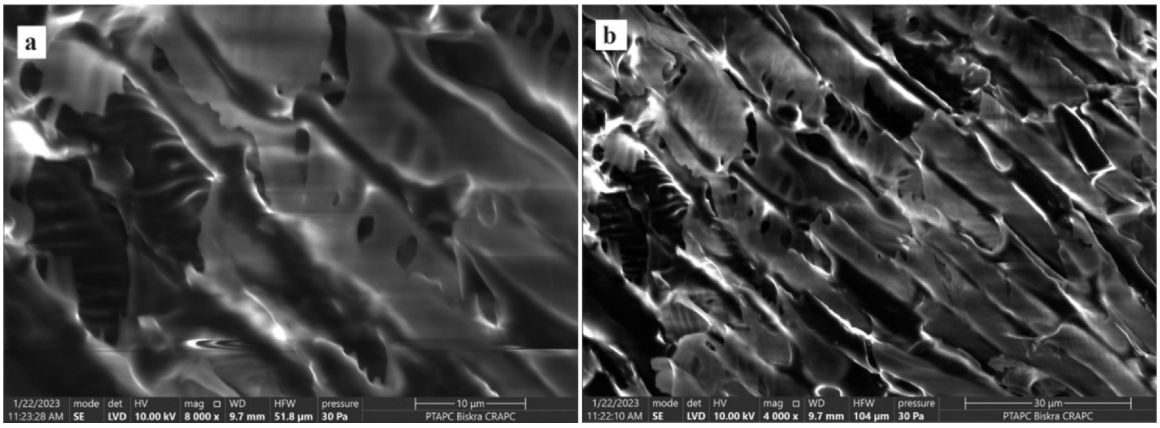

Fig. 3. SEM images of Silybum marianum seed shells at (a) 10 µm, and (b) 30 µm.

its complex molecular structure [21]. The DTA diagrams of SMSS particles exhibit discernible exothermic peaks, signifying distinct degradation reactions. The first peak at 80 °C is attributed to the evaporation of absorbed water. Subsequently, the second peak observed at 280 °C correlates with the degradation of hemicelluloses. The third peak, at 350 °C, corresponds to the decomposition of cellulose, resulting in the generation of volatile products [22]. The last peak, registered at 500 °C, is attributed to the oxidation of these volatile products.

3.1.5. Specific surface area

Specific surface area can play a crucial role for the adsorption ability depending on the type of pollutant. The specific surface area of SMSS was evaluated using nitrogen gas (N_2) at a temperature of 77.3 K. The results are represented in Table 1. The examination revealed that the material exhibits microporous attributes follow the criteria established by IUPAC [23]. The specific surface area was determined to be approximately 1.47 m^2/g, accompanied by a pore diameter of 15.28 Å. Noteworthy is the observation that the identified pore diameter surpasses that of BF molecules, which have a diameter of approximately 11.34 Å. Consequently, it could easily infiltrate the microstructure of the material. The adsorption of pollutants on the surface of adsorbent depends on several factors. Indeed the surface area is crucial factor, however, the affinity between the adsorbent and the pollutant, which is governed by electrostatic forces, could be considered as the most important step in adsorption. In fact, the surface of lignocellulose-based adsorbents such as SMSS is very rich with different functional groups which boost the fixation of charged dye molecules. It is important to point out that SMSS was used without carbonization, nor chemical activation steps to avoid the high cost of these processes. The carbonization and chemical/physical activation is the main factor to enhance the surface area and the porosity.

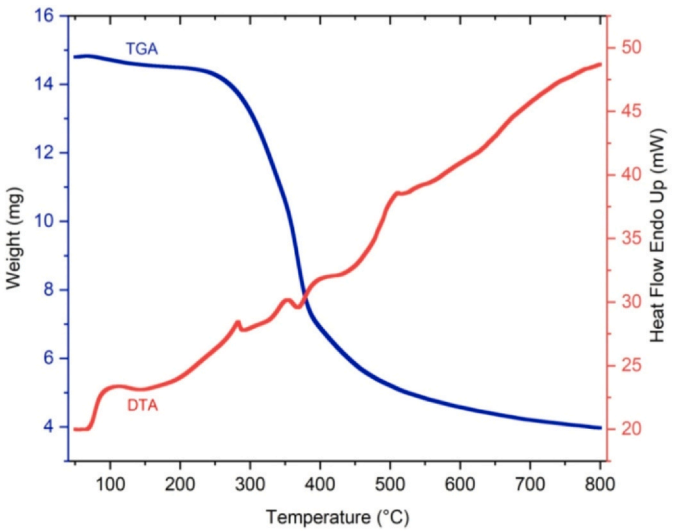

Fig. 4. TGA-DTA curves of *Silybum marianum* seed shells.

3.2. Batch adsorption experiments

3.2.1. Effect of particle size

The size of biosorbent particles plays a crucial role in determining their adsorption capacity. This study examined four different particle sizes and analyzed their efficacy in removing BF dye. Fig. 5 illustrates the relation between the removal efficiency of BF dye and biosorbent particle size. It was found that the most effective size of SMSS for BF removal ranged between 250 and 500 µm. Based on these findings, subsequent experiments were conducted using SMSS particles within this size range.

3.2.2. Effect of biosorbent mass

Numerous experiments were conducted to determine the optimal dose of SMSS for removing BF dye from aqueous solutions. The influence of biosorbent mass on the efficiency of BF dye removal is illustrated in Fig. 6. The study concluded that the adsorption efficiency of BF dye increases with higher doses of SMSS. This is attributed to the increased availability of active adsorptive sites [24,25]. However, the removal rate attains stability at a saturation point beyond a dosage of 5 g/L, wherein the optimal dye adsorption rate of 95.11% was achieved. Consequently, based on these findings, 5 g/L was identified as the optimal dosage for achieving the utmost BF dye adsorption efficiency.

3.2.3. Effect of stirring speed

The stirring speed plays a critical role during adsorption, particularly for dye adsorption, as it directly influences solute distribution in the solution [26]. Therefore, three different stirring speeds were tested: 50, 100, and 150 rpm. Fig. 7 shows that an increase in stirring speed enhances BF adsorption. This can be attributed to the fact that the rise in speed increases the transfer of BF ions to the SMSS. Furthermore, the figure shows that the higher adsorption efficiency, i.e., 95.55%, was achieved at a stirring speed of 150 rpm.

Table 1
Physical properties of SMSS.

Characteristics	Surface Area (m^2/g)	Pore Volume (cc/g)	Pore Radius (Å)
SMSS	1.470	0.002	15.283

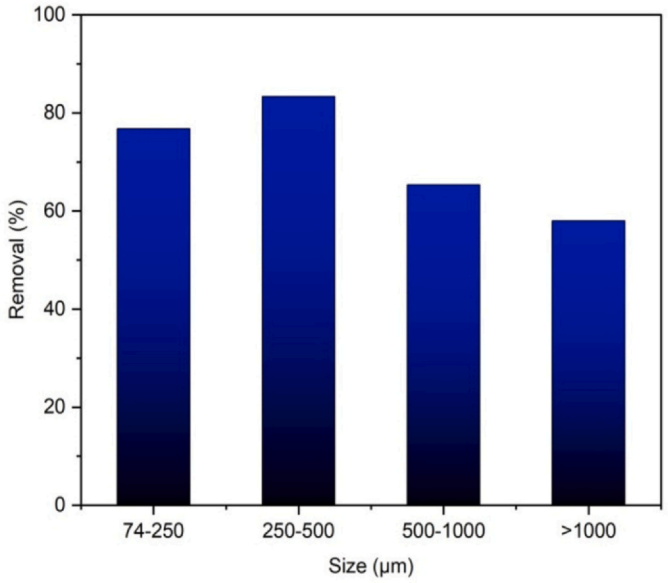

Fig. 5. SMSS Particle size effect on BF dye removal ([BF] = 10 mg/L; t = 60 min; [SMSS] = 3 g/L; Original pH = 6.9; T: 25 °C).

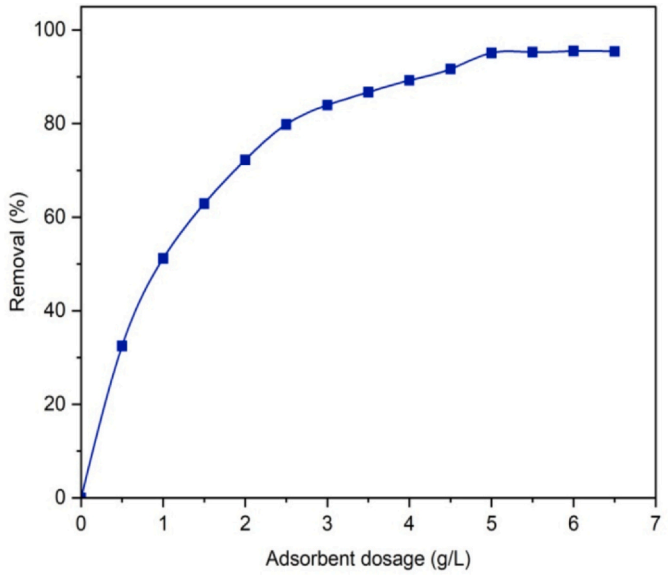

Fig. 6. biosorbent mass effect on BF dye removal ([BF] = 10 mg/L; t = 60 min; SMSS particle size: [250 − 500] μm; Original pH = 6.9; T = 25 °C).

3.2.4. Effect of initial BF concentration

A series of experiments were conducted to explore the impact of the initial dye concentration on the adsorption efficiency of BF dye. Four different concentrations were examined, namely 10, 20, 30, and 40 mg/L. Fig. 8 illustrates the correlation between the initial dye concentration and the adsorption efficiency of BF dye. The findings indicate that the optimum removal efficiency occurred when the initial dye concentration was 10 mg/L. However, as the concentration increased from 10 to 40 mg/L, there was a slight reduction in efficiency, possibly attributable to the insufficient availability of active sites resulting from higher sorption of dye molecules [27].

3.2.5. Effect of temperature

To investigate the influence of temperature on the adsorption process, we conducted a study at three distinct temperatures: 25 °C, 35 °C, and 45 °C. The results presented in Fig. 9 reveal that elevating the temperature from 25 °C to 35 °C or 45 °C enhances the speed of BF adsorption, potentially attributed to the heightened mobility of BF ions [28]. Additionally, it is acknowledged that the diffusion rate of dye molecules through the outer boundary layer and into the biosorbent particles increases with increasing temperature [29].

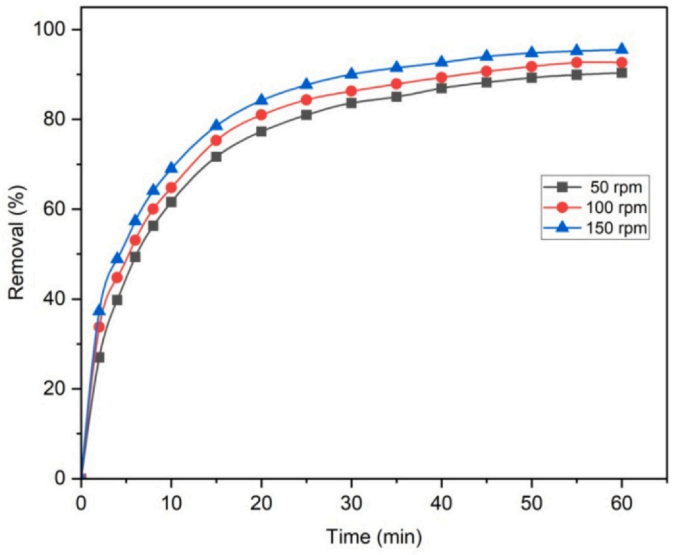

Fig. 7. Stirring speed effect on BF dye removal ([BF] = 10 mg/L; SMSS particle size: [250 − 500] μm; [SMSS] = 5 g/L; Original pH = 6.9; T = 25 °C).

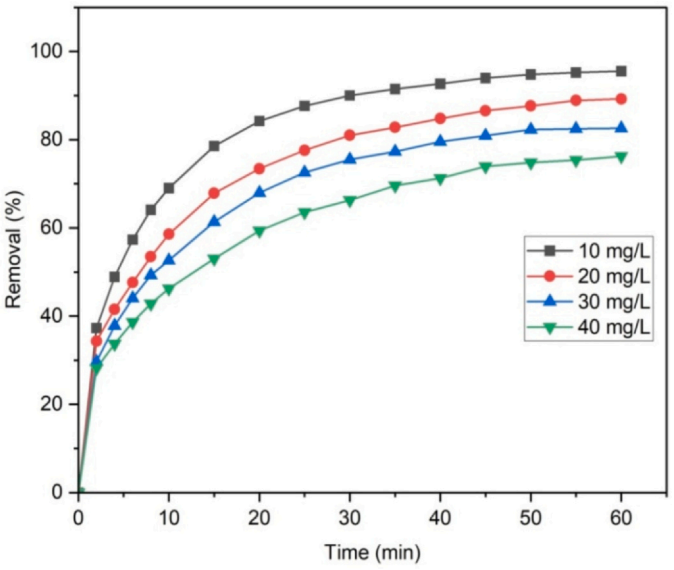

Fig. 8. Initial dye concentration effect on BF dye removal (SMSS particle size: [250 − 500] μm; [SMSS] = 5 g/L; Stirring speed = 150 rpm; Original pH = 6.9; T = 25 °C).

3.2.6. Effect of solution pH

Examining the impact of solution pH on the adsorption process is crucial for comprehending the experimental outcomes in a complex environment. To this end, experiments were carried out by adjusting the pH of the dye solution within the range of 2 to 12. As depicted in Fig. 10, the adsorption efficiency of BF dye is significantly influenced by acidic environments (pH = 2). However, with an increase in pH, the adsorption efficiency gradually improves, reaching its peak at pH 12 with an impressive efficiency rate of 97.50%. This indicates that an

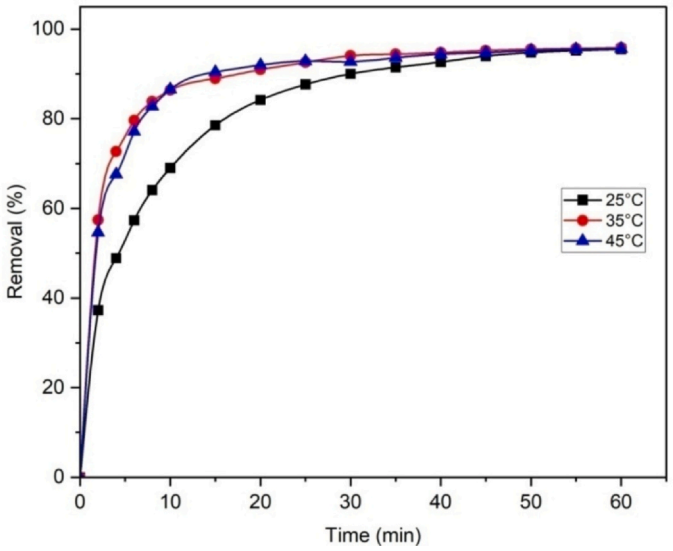

Fig. 9. Temperature effect on BF dye removal ([BF] = 10 mg/L; SMSS particle size: [250 − 500] µm; [SMSS] = 5 g/L; Stirring speed = 150 rpm; Original pH = 6.9).

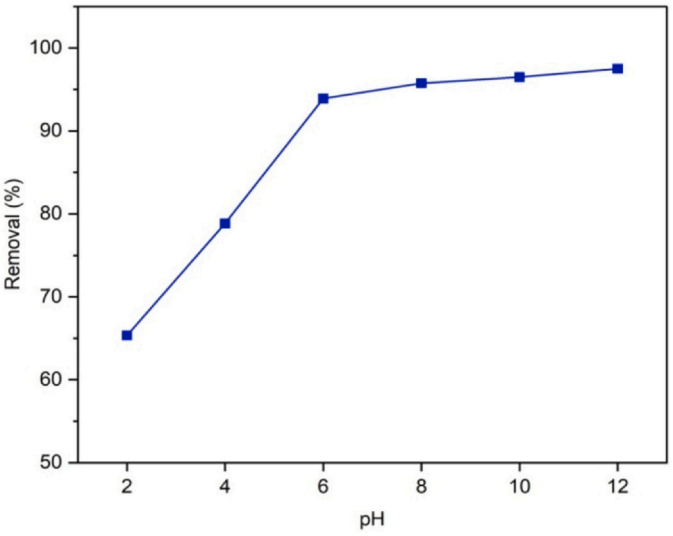

Fig. 10. pH effect on BF dye removal ([BF] = 10 mg/L; t = 60 min; SMSS particle size: [250 − 500] µm; [SMSS] = 5 g/L; Stirring speed = 150 rpm; T = 25 °C).

elevation in pH favors the formation of groups such as $R - NH^-$, $R - CO - NH^-$, $R - O^-$, $R - COO^-$, resulting in an augmentation of negative charges on the surface of SMSS. This facilitates the electrostatic attraction of BF (R^+, Cl^-) due to its positive charges in the solution [30], as illustrated by the following equations:

$$R - NH_2 + OH^- \rightarrow R - NH^- + H_2O$$

$$R - CO - NH_2 + OH^- \rightarrow R - CO - NH^- + H_2O$$

$$R - OH + OH^- \rightarrow R - O^- + H_2O$$

$$R - COOH + OH^- \rightarrow R - COO^- + H_2O$$

Under acidic pH conditions, however, these groups undergo protonation, causing the surface to acquire a positive charge [31]. This positive charge results in electrostatic repulsion with BF dye, obstructing adsorption. This is better clarified through the following reactions:

$$R - NH_2 + H^+ \rightarrow R - NH_3^+$$

$$R - CO - NH_2 + H^+ \rightarrow R - CO - NH_3^+$$

$$R - OH + H^+ \rightarrow R - OH_2^+$$

$$R - COOH + H^+ \rightarrow R - COOH_2^+$$

3.2.7. Effect of natural water matrices

The investigation into the effects of both inorganic and organic compounds present in a real sample on the adsorption of dyes is of particular interest. Therefore, different water samples were selected for this experiment; distilled water was prepared in our laboratory, a seawater sample was obtained from the Mediterranean Sea, a tap water sample was taken in our laboratory after opening the tap for 10 min, and mineral water obtained from the Biskra region south of the Aures. The Physicochemical parameters of the different samples are presented in Table 2. Basic fuchsine was dissolved in each water sample to perform the adsorption experiments. Fig. 11 displays the adsorption efficiency of BF dye for the different water samples. The highest adsorption rate was 95.52%, obtained using distilled water. The adsorption efficiencies using tap and mineral water were 84.42% and 83.68%, respectively. However, in terms of seawater case, the adsorption efficiency was significantly affected, with a rate removal of 63%. This indicates that various inorganic and organic substances can interact with SMSS, especially chlorine and sulfate ions, which tend to bind to the biosorbent surface and cover the active sites of the used material. The findings suggest that the adsorption process is adversely impacted by the presence of other compounds in the reaction medium, which aligns with previous studies results [32].

3.3. Kinetics modeling

The validity of the pseudo-first-order model is assessed by plotting ln ($q_e - q_t$) against t. From Fig. 12 (a), depicting the pseudo-first-order kinetics for BF dye during the adsorption process and the corresponding parameters detailed in Table 3, it can be seen that the (R^2) values are relatively low. Additionally, a disparity exists between the experimental

Table 2
Physicochemical parameters of natural water matrices.

water matrices	Physicochemical parameters									
	pH	EC5 µs/cm	TDS mg/L	Ca^{2+} mg/L	Mg^{2+} mg/L	K^+ mg/L	Cl^- mg/L	SO_4^{2-} mg/L	HCO_3^- mg/L	NO_3^- mg/L
Distilled Water	7.1	1.05	0	0.01	0.05	0	0.71	0	3	0
Tap Water	7.58	387	277	76	38.4	3.2	49	187.2	124	2.66
Mineral Water	7.50	819.5	654.75	54	35	2.4	70.91	108.09	305.1	4.67
Sea water	7.8	55400	35200	200	780.8	148.8	6816	1260	132.5	5.9

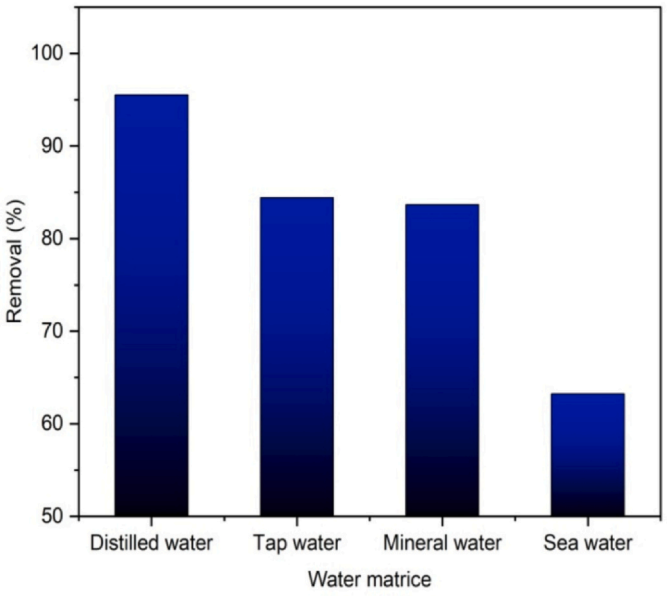

Fig. 11. Natural water matrices effect on BF dye removal ([BF] = 10 mg/L; t = 60 min; SMSS particle size: [250 − 500] μm; [SMSS] = 5 g/L; Stirring speed = 150 rpm; Original pH = 6.9; T = 25 °C).

and calculated (q_e) values. Conversely, as illustrated in Fig. 12 (b) for the pseudo-second-order model and the associated parameters in Table 3, the (R^2) values are higher and more fitting. The findings suggest that the adsorption of BF dye onto SMSS adheres to the pseudo-second-order model.

3.4. Isotherms modeling

Examining adsorption isotherms enhances our comprehension of dye/biosorbent interactions and aids in identifying the nature of adsorption. Fig. 13 illustrates the adsorption isotherm of BF dye onto SMSS. The results indicate that the adsorption isotherm aligns with Type L per the Giles classification [33]. The experimental data were further scrutinized using the Freundlich and Langmuir isotherm models, as shown in Fig. 14. Through an evaluation of the isotherm parameters and correlation coefficients (R^2) summarized in Table 4, and the presentation of the Langmuir model in its linear form in Fig. 14 (b), it was determined that the Langmuir model provided the most fitting representation for the adsorption of BF dye onto SMSS.

3.5. Thermodynamic study

Table 5 provides the thermodynamic parameters corresponding to the adsorption of BF dye onto SMSS at various temperatures. The negative values of the change in Gibbs free energy (ΔG°) (−4.730, −7.144, and −6.856 KJ/mol at 298, 308, and 318 K, respectively) signify the feasibility and spontaneity of the adsorption process for BF dye. Furthermore, these ΔG° values indicate that the adsorption

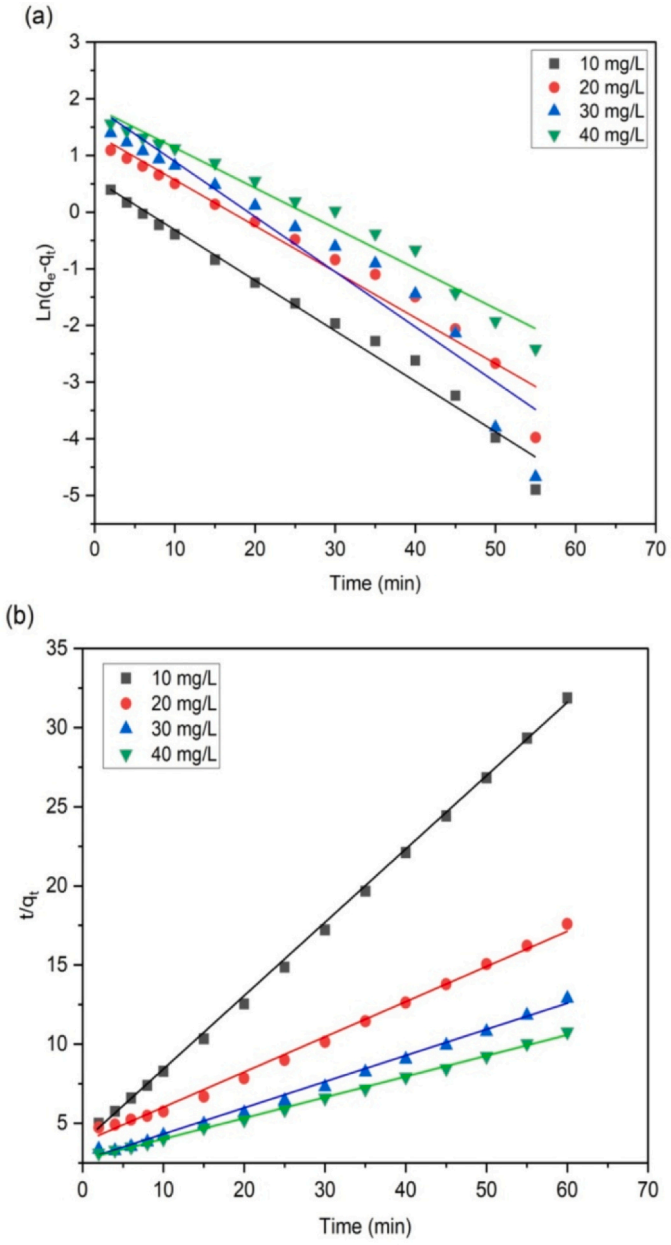

Fig. 12. Line graphs of (a) the Pseudo-first order model, and (b) the Pseudo-second-order model for BF adsorption process onto SMSS.

Table 3
Kinetic parameters of the adsorption of basic fuchsin onto SMSS.

Kinetic Model		Basic fuchsin concentration (mg/L)			
		10	20	30	40
Pseudo-first order	q_e	1.777	4.051	6.82	6.41
	K_1	0.089	0.081	0.1	0.071
	R^2	0.981	0.958	0.926	0.975
Pseudo-second order	q_e	2.159	4.444	6.024	7.633
	K_2	0.059	0.013	0.01	0.006
	R^2	0.999	0.995	0.995	0.998
$q_e$exp (mg/g)		1.882	3.411	4.657	5.564

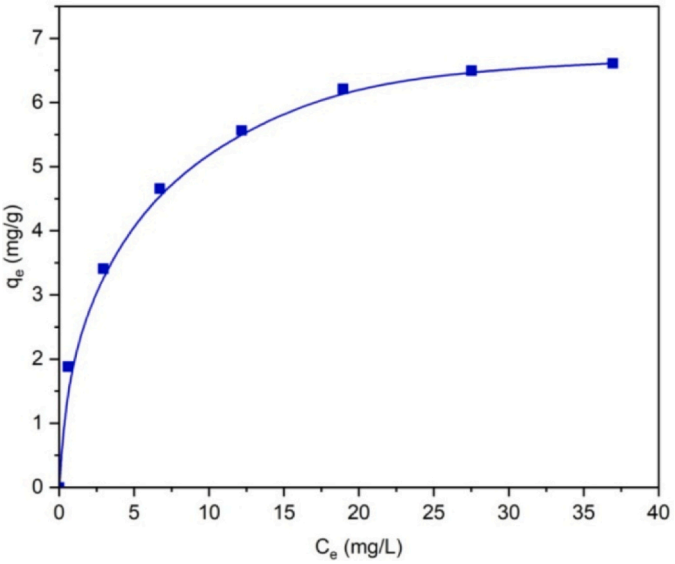

Fig. 13. Adsorption isotherm of BF dye on SMSS.

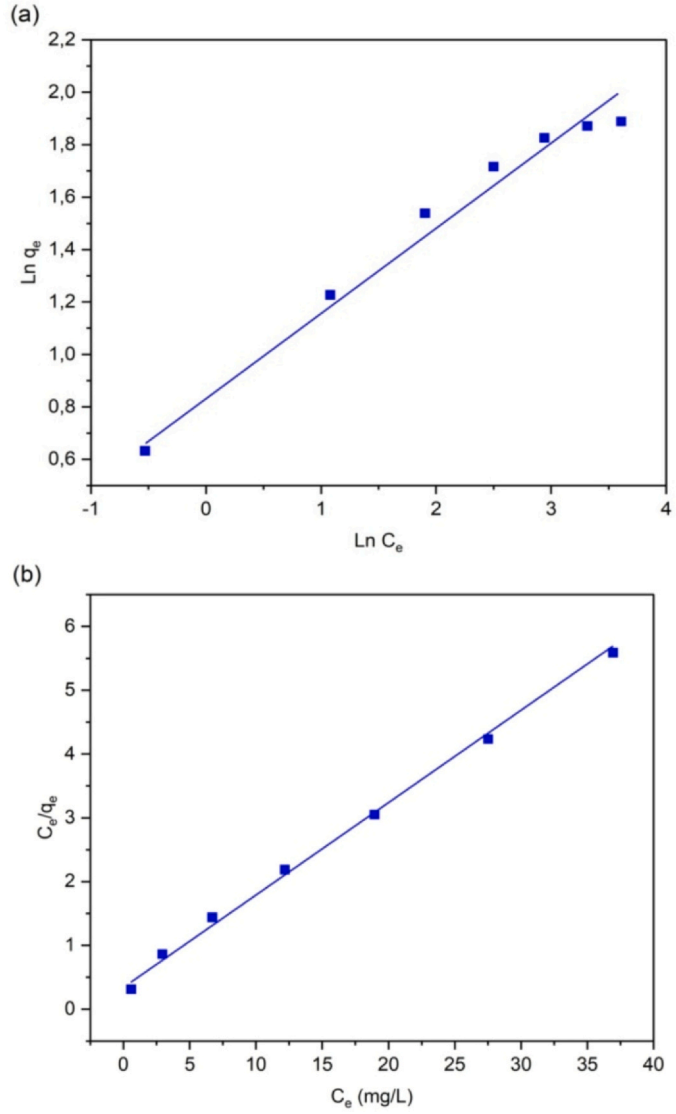

Fig. 14. (a) the Freundlich isotherm and (b) the Langmuir isotherm of BF dye adsorption onto SMSS.

Table 4
Parameters of Freundlich and Langmuir isotherms for BF dye adsorption onto SMSS.

Isotherm	Parameters	Values
Freundlich	K_f (L/mg)	2.377
	N	3.194
	R^2	0.976
Langmuir	K_L (L/mg)	0.353
	q_m (mg/g)	7.142
	R^2	0.997

Table 5
Thermodynamic parameters of the adsorption of BF dye onto SMSS at different temperatures.

T (K)	ΔG° (kJ/mol)	ΔH° (kJ/mol)	ΔS° (kJ/mol.K)
298	-4.730	67.218	0.2414
308	-7.144		
318	-6.856		

Table 6
Comparison of adsorption efficiency of BF onto various adsorbents.

Adsorbent	Experimental conditions	Removal yield	Reference
Raw Pistachio Nutshells (RPNS)	[BF] = 30 mg/L; [RPNS] = 4 g/L; pH = 9; t = 30 min; T = 25 °C	96.45%	[35]
Carica papaya seeds (CPS)	[BF] = 50 mg/L; [CPS] = 6 g/L; pH = 11; t = 180 min; T = 25 °C	95%	[36]
Euryale ferox Salisbury seed shell (E. ferox)	[BF] = 40 mg/L; [E. ferox] = 40 g/L; pH = 6; t = 120 min; T = 30 °C	97.4%	[37]
Mandacaru (*Cereus jamacaru)* leaves (PML)	[BF] = 100 mg/L; [PML] = 0.0375 g/L; pH = 8; t = 150 min; T = 55 °C	90%	[38]
Calcined mussel shells (CMS)	[BF] = 60 mg/L; [CMS] = 5 g/L; pH = 9; t = 240 min; T = 25 °C	90%	[39]
Silybum marianum seed shells (SMSS)	[BF] = 10 mg/L; [SMSS] = 5 g/L; pH = 12; t = 60 min; T = 25 °C	97.5%	This study

of BF dye is predominantly a physical process since a physisorption process takes place within the range of [− 20 to 0.0] kJ/mol and a chemisorption process within the range of [− 80 to − 400] kJ/mol [34]. On the other hand, the positive values of ΔH° and ΔS° (Table 5) suggest that the adsorption process is endothermic. Table 6.

4. Conclusion

The findings of this study demonstrate the efficacy of *Silybum marianum* seed shells (SMSS) as a proficient biosorbent for eliminating basic fuchsin (BF) dye from aquatic ecosystems. The lignocellulosic fibrous structure of SMSS, characterized by high porosity, contributes to its outstanding

adsorption efficiency. The adsorption of BF dye was notably influenced by the dosage of SMSS, initial dye concentration, and solution pH. Under optimized conditions, an impressive 97.50% removal efficiency was achieved, underscoring the potential of SMSS as a cost-effective and environmentally friendly alternative for water treatment. The adsorption kinetics aligned well with the pseudo-second-order model, while the equilibrium data demonstrated a good fit with the Langmuir isotherm. The thermodynamic study indicated that the adsorption process of BF dye onto SMSS is endothermic. In conclusion, this study provides valuable insights into the biosorption behavior of SMSS concerning BF dye and highlights its promising applications in water treatment.

Declaration of Competing Interest

The authors declare that they have no known competing financial interests or personal relationships that could have appeared to influence the work reported in this paper.

Acknowledgement

Authors thank the MESRS for their collaboration in providing the necessary funding.

References

[1] Djellabi R, Ghorab MF. Solar photocatalytic decolourization of Crystal violet using supported TiO_2: effect of some parameters and comparative efficiency. Desalin Water Treat 2015;53(13):3649–55.
[2] Hamdaoui O, Saoudi F, Chiha M, Naffrechoux E. Sorption of malachite green by a novel sorbent, dead leaves of plane tree: Equilibrium and kinetic modeling. Chem Eng J 2008;143(1-3):73–84.
[3] Merouani S, Hamdaoui O. Computational and experimental sonochemistry. Process Eng J 2017;1:10–8.
[4] Ali J, Wang L, Waseem H, Djellabi R, Oladoja NA, Pan G. FeS@ rGO nanocomposites as electrocatalysts for enhanced chromium removal and clean energy generation by microbial fuel cell. Chem Eng J 2020;384:123335.
[5] Haider MR, Jiang WL, Han JL, Mahmood A, Djellabi R, Liu H, et al. Boosting hydroxyl radical yield via synergistic activation of electrogenerated HOCl/H2O2 in electro-fenton-like degradation of contaminants under chloride conditions. Environ Sci Technol 2023.
[6] Saeedi-Jurkuyeh A, Jafari AJ, Kalantary RR, Esrafili A. A novel synthetic thin-film nanocomposite forward osmosis membrane modified by graphene oxide and polyethylene glycol for heavy metals removal from aqueous solutions. React Funct Polym 2020;146:104397.
[7] Xia J, Lei X, Lu Y, Liu S, Luo X. Coagulation mechanism of cellulose/metal nanohybrids through a simple one-step process and their interaction with Cr (VI). Int J Biol Macromol 2020;142:404–11.
[8] Li R, Hu D, Hu K, Deng H, Zhang M, Wang A, et al. Coupling adsorption-photocatalytic reduction of Cr (VI) by metal-free N-doped carbon. Sci Total Environ 2020;704:135284.
[9] Nouacer S, Djellabi R. Easy-handling semi-floating TiO2-based aerogel for solar photocatalytic water depollution. Environ Sci Pollut Res 2023;30(9):22388–95.
[10] Mergbi M, Galloni MG, Aboagye D, Elimian E, Su P, Ikram BM, et al. Valorization of lignocellulosic biomass into sustainable materials for adsorption and photocatalytic applications in water and air remediation. Environ Sci Pollut Res 2023:1–31.
[11] Abderrahim N, Mergbi M, Amor HB, Djellabi R. Optimization of microwave assisted synthesis of activated carbon from biomass waste for sustainable industrial crude wet-phosphoric acid purification. J Clean Prod 2023;394:136326.
[12] Lagergren SK. About the theory of so-called adsorption of soluble substances. Sven Vetensk Handingarl 1898;24:1–39.
[13] Ho YS, McKay G. Pseudo-second order model for sorption processes. Process Biochem 1999;34(5):451–65.
[14] Fu J, Chen Z, Wang M, Liu S, Zhang J, Zhang J, et al. Adsorption of methylene blue by a high-efficiency adsorbent (polydopamine microspheres): kinetics, isotherm, thermodynamics and mechanism analysis. Chem Eng J 2015;259:53–61.
[15] Song K, Xu H, Xu L, Xie K, Yang Y. Cellulose nanocrystal-reinforced keratin bioadsorbent for effective removal of dyes from aqueous solution. Bioresour Technol 2017;232:254–62.
[16] Elkady MF, Ibrahim AM, Abd El-Latif MM. Assessment of the adsorption kinetics, equilibrium and thermodynamic for the potential removal of reactive red dye using eggshell biocomposite beads. Desalination 2011;278(1-3):412–23.
[17] Kumari HJ, Krishnamoorthy P, Arumugam TK, Radhakrishnan S, Vasudevan D. An efficient removal of crystal violet dye from waste water by adsorption onto TLAC/Chitosan composite: a novel low cost adsorbent. Int J Biol Macromol 2017;96:324–33.
[18] Lahmar A, Hattab Z, Zerdoum R, Berredjem A, Djellabi R, Guerfi K. Removal of basic fuchsin from aqueous solutions by low-cost peanut shells adsorbent in a fixed bed column. Desalin Water Treat 2020;191:400–16.
[19] Foroutan R, Peighambardoust SJ, Aghdasinia H, Mohammadi R, Ramavandi B. Modification of bio-hydroxyapatite generated from waste poultry bone with MgO for purifying methyl violet-laden liquids. Environ Sci Pollut Res 2020;27:44218–29.
[20] Essabir H, Hilali E, Elgharad A, El Minor H, Imad A, Elamraoui A, et al. Mechanical and thermal properties of bio-composites based on polypropylene reinforced with Nut-shells of Argan particles. Mater Des 2013;49:442–8.
[21] KifaniSahban F, Belkbir L, Zoulalian A. Study of the slow pyrolysis of moroccan eucalyptus by thermal-analysis. Thermochim Acta 1996;284(2):341–9.
[22] Sefain MZ, El-Kalyoubi SF. Thermogravimetric studies of different celluloses. Thermochim Acta 1984;75(1-2):107–13.
[23] An FH, Cheng YP, Wu DM, Wang L. The effect of small micropores on methane adsorption of coals from Northern China. Adsorption 2013;19:83–90.
[24] Nandi BK, Goswami A, Purkait MK. Adsorption characteristics of brilliant green dye on kaolin. J Hazard Mater 2009;161(1):387–95.
[25] Nandi BK, Goswami A, Purkait MK. Removal of cationic dyes from aqueous solutions by kaolin: kinetic and equilibrium studies. Appl Clay Sci 2009;42(3-4):583–90.
[26] Crini G, Badot PM. Application of chitosan, a natural aminopolysaccharide, for dye removal from aqueous solutions by adsorption processes using batch studies: a review of recent literature. Prog Polym Sci 2008;33(4):399–447.
[27] Yang Y, Ali N, Khan A, Khan S, Khan S, Khan H, et al. Chitosan-capped ternary metal selenide nanocatalysts for efficient degradation of Congo red dye in sunlight irradiation. Int J Biol Macromol 2021;167:169–81.
[28] Mellah A, Chegrouche S. The removal of zinc from aqueous solutions by natural bentonite. Water Res 1997;31(3):621–9.
[29] Srivastava VC, Mall ID, Mishra IM. Characterization of mesoporous rice husk ash (RHA) and adsorption kinetics of metal ions from aqueous solution onto RHA. J Hazard Mater 2006;134(1-3):257–67.
[30] Manera C, Tonello AP, Perondi D, Godinho M. Adsorption of leather dyes on activated carbon from leather shaving wastes: kinetics, equilibrium and thermodynamics studies. Environ Technol 2018.
[31] Bessashia W, Berredjem Y, Hattab Z, Bououdina M. Removal of Basic Fuchsin from water by using mussel powdered eggshell membrane as novel bioadsorbent: equilibrium, kinetics, and thermodynamic studies. Environ Res 2020;186:109484.
[32] De Laat J, Le TG. Effects of chloride ions on the iron (III)-catalyzed decomposition of hydrogen peroxide and on the efficiency of the Fenton-like oxidation process. Appl Catal B: Environ 2006;66(1-2):137–46.
[33] Ch G. Studies in adsorption. Part XI. A system of classification of solution adsorption isotherms, and its use in diagnosis of adsorption mechanisms and in measurements of specific surface areas of solids. J Chem Soc 1960;786:3973–93.
[34] Li Y, Du Q, Liu T, Sun J, Wang Y, Wu S, et al. Methylene blue adsorption on graphene oxide/calcium alginate composites. Carbohydr Polym 2013;95(1):501–7.
[35] El-Azazy M, El-Shafie AS, Ashraf A, Issa AA. Eco-structured biosorptive removal of basic fuchsin using pistachio nutshells: A definitive screening design—based approach. Appl Sci 2019;9(22):4855.
[36] Gaye AA, Ayessou NC. Bio-sorption of methylene blue and basic fuchsin from aqueous solution onto defatted Carica papaya seeds: Mechanism and effect of operating parameters on the adsorption yield. IOSR J Environ Sci, Toxicol Food Technol 2020;13:24–33.
[37] Kalita S, Pathak M, Devi G, Sarma HP, Bhattacharyya KG, Sarma A, et al. Utilization of euryale ferox salisbury seed shell for removal of basic fuchsin dye from water: equilibrium and kinetics investigation. R Soc Chem Adv 2017;7(44):27248–59.
[38] Georgin J, Franco D, Drumm FC, Grassi P, Netto MS, Allasia D, et al. Powdered biosorbent from the mandacaru cactus (Cereus jamacaru) for discontinuous and continuous removal of Basic Fuchsin from aqueous solutions. Powder Technol 2020;364:584–92.
[39] El Haddad M. Removal of basic fuchsin dye from water using mussel shell biomass waste as an adsorbent: equilibrium, kinetics, and thermodynamics. J Taibah Univ Sci 2016;10(5):664–74.